Ion Temperature Gradient Driven Transport

W. Horton

Institute for Fusion Studies, The University of Texas at Austin

Austin, Texas 78712

Abstract

The steep ion temperature gradients produced in the large tokamaks are analyzed in terms of the anomalous transport of ion energy and momentum. The transport equations take into account that for low viscosities and high effective Rayleigh numbers both neutral fluids and plasma show the spontaneous generation of sheared mass flows. The self-generated flows are driven by the ion temperature gradient through the turbulence and are one method for creating the transport barrier. In addition, the external control parameter from the direct injection of perpendicular ion (angular) momentum gives a second method for creating a transport barrier. The threshold conditions are derived for the bifurcations from the three confinement regimes of L-mode, H-mode, and a super-suppressed transport (SST) confinement regime.

International Symposium in Honor of Bruno Coppi
January 19-20, 1995, Massachusetts Institute of Technology

I. INTRODUCTION

In the large tokamaks ($R \gtrsim 2\,\mathrm{m}$, $B \gtrsim 2\,\mathrm{T}$, $I > 1\,\mathrm{MA}$) strong auxiliary heating is applied with multiple neutral beam lines and radio frequency heating that provide controllable energy and (angular) momentum deposition profiles. In the highest power experiments[1,2] the local power deposition is of order one megawatt per cubic meter which drives up ion temperature gradients on the order of $40\,\mathrm{kV/m}$. In addition strongly sheared ion mass flows are observed both in the toroidal and poloidal directions.[1,2]

The standard model for the analysis of the ion power balance in these regimes is the ion thermal conductivity χ_i arising from the ion temperature gradient itself. While turbulent thermal conductivity formulas necessarily have some uncertainties in them due to the nature of turbulence, there are well-agreed-upon general features of the χ_i formula that has evolved over the past ten years from a combination of theory and computer simulations.

Important features of the ion thermal conductivity formula confirmed by simulations arise from the linear and quasilinear theories. The first comprehensive analysis of the ion temperature gradient driven instability and quasilinear estimate of its transport is given by Coppi-Rosenbluth-Sagdeev.[3] This work analyzes the wave functions and the eigenvalues in the sheared slab magnetic field geometry and shows the remarkable feature that the growth rate increases with increasing magnetic shear $S = L_n/L_s$ for low values of S. As the magnetic shear increases, however, the mode width Δx decreases according to $\Delta x = \rho_s(L_s/L_n)^{1/2}$ so that both the mixing length estimate $\gamma \Delta x^2$ and the quasilinear theory for χ_i show a weak decreasing thermal conductivity with increasing magnetic shear strength. Horton *et al.*[4] carried out 3D FLR-fluid simulations to investigate the dependence of χ_i on the magnetic shear parameter and $\eta_i = \partial_x \ell n T_i / \partial_x \ell n n = L_n/L_{Ti}$ parameter and compared their result with scaling estimate of Coppi *et al.*[3] The exact form of the magnetic shear dependence has been a strongly debated issue and for the shear slab problem both the global $\chi_i(S)$ and the local scaling forms $\chi_0 S^{-\alpha}$ are given in Hamaguchi and Horton for order unity[5] and large η_i regimes.[6]

A second major advance was made in extending the analysis of ∇T_i driven modes into toroidal geometry by Coppi and Pegoraro[7] using both fluid and kinetic descriptions of the linear fluctuations in a torus. Subsequently, Coppi, Migliuolo, and Pu (1990) re-examined the stability analysis numerically and, in addition, calculated the quasilinear particle and thermal fluxes.[7]

In the toroidal geometry the grad-B and curvature drifts produce an unfavorable charge separation in the fluctuations on the outside of the torus and a favorable (stabilizing) separation on the inside. The eigenmode problem becomes the classic one of finding the periodic solutions in a sheared toroidal magnetic field. The potential for the local flute-like modes contains the effective gravity of the form $\omega_D(\theta)/\omega_* = (2L_n/R)(\cos\theta + s\theta\sin\theta)$ where θ is the poloidal angle, $\varepsilon_n = L_n/R$ is the strength of the toroidicity and $s = rq'/q$ is the reduced shear parameter ($L_s = qR/s$). Here again Coppi was one of the first to recognize the general importance of solving such toroidal eigenvalue problems.[8] Coppi gave the procedure for constructing what he called the "disconnected modes" that are the strongly ballooning modes[8] now seen in the global particle simulations of LeBrun *et al.*[9] and Parker *et al.*[10] The growth rate and thermal diffusivities for the strongly growing modes increase as $(L_n/R)^{1/2}$ thus giving the strong enhancement of the toroidal ion temperature gradient transport over the corresponding slab transport. The transition from the slab to the toroidal regimes is now well documented in simulations[9–10,15] and analyzed theoretically by Kim and Horton.[11]

Let us turn to the analytic model of the toroidal ion thermal diffusivity. Horton-Choi-Tang[12] (hereafter HCT) use the ballooning eigenmodes parameterized by ε_n, η_i, q and s to determine both the linear mode features $\Delta x, \gamma_k, \Delta\theta$ and to reduce the mode coupling equations to a form containing the principal $\mathbf{E}\times\mathbf{B}$ mixing nonlinearity. With the quasinormal approximation and the short correlation time (Markovianization) HCT derive the wave-kinetic equation governing the spectral density $I(\mathbf{k}) = \langle|\varphi_{\mathbf{k}}|^2\rangle$ and give approximate solutions for $I(k_y) = \int dk_x\, I(k_x, k_y)$ and the associated thermal conductivity $\chi^{\mathrm{HCT}}(\eta_i, s/q, \varepsilon_n)$.

II. ION THERMAL CONDUCTIVITY

HCT investigated the toroidal ion temperature gradient $\eta_i = L_n/L_{Ti}$ and the toroidicity parameter $\varepsilon_n = L_n/R$ driven turbulence using a reduced set of mode coupling equations. The two key steps in the reduction were (1) to use the ballooning mode or "disconnected mode" approximation for the mean value of $\langle k_x^2\rangle$ thus reducing the nonlinear spectral problem to an integral equation for the 1D spectrum $I(k_y) = \int dk_x \left\langle|\varphi_{\mathbf{k}}|^2\right\rangle$ with $\gamma_k = (c_s/L_n)(k\rho_s)\sqrt{2\varepsilon_n(\eta_i - \eta_{\mathrm{crit}})}$ as the driver and (2) to retain only the nonlinearity from the convective derivative of the pressure. The HCT formula for χ_i is

$$\chi_i = \frac{\rho_i q}{L_n s}\left(\frac{cT_e}{eB}\right)\left[2\varepsilon_n(\eta_i - \eta_{\mathrm{crit}})\right]^{1/2} \tag{1}$$

where the threshold value η_{crit} of the temperature gradient must be taken from later kinetic theory calculations such as that from Kim and Horton[13] giving

$$\left.\frac{L_n}{T_i}\frac{dT_i}{dx}\right)_{\mathrm{crit}} = \eta_{\mathrm{crit}} = \frac{2}{3} + \frac{4L_n}{3R}\left(1 + \frac{T_i}{T_e}\right) \tag{2}$$

or from Romanelli.[14]

Recently, extensive numerical simulations at the IFS have led to a more complete and complex parameterization of the χ_i formula and the threshold function.[15] A simplified form of the full formula (that contains twenty numerical parameters) is

$$\chi_i \cong \frac{7q\rho_i}{1+s/2}\left(\frac{cT_e}{eB}\right)\left(\frac{1}{L_{T_i}} - \frac{1}{L_{T_i,\mathrm{crit}}}\right) \tag{3}$$

where

$$\left(\frac{1}{L_{T_i}}\right)_{\mathrm{crit}} = \frac{2}{R}\left(1 + \frac{2}{q}\right)\left(\frac{T_i}{T_e}\right)^{2/3}\left[1 + \frac{s^2}{2} + \left(\frac{R}{L_n}\right)^{2/3}\right]. \tag{4}$$

A complicated Z_{eff} function is omitted for reasons discussed below.

The formula for $L_{T_i,\text{crit}}$ is of much importance since it determines the marginal stability profile as can be seen by integrating Eq. (2) or Eq. (3) across the plasma radius. The T_i dependence on the right-hand side of Eq. (2) gives a sharp increase in the core of the marginal stability $T_i^{\text{ms}}(x)$ profile as easily worked out in detail by integrating the first order nonlinear equation given by Eq. (2). Fortunately, the value of $L_{T_i,\text{crit}}$ is determined by the marginal stability analysis of the linear dispersion relation or by repeated runs of initial value simulations to determine $L_{T_i,\text{crit}}$ as a function of system parameters.[15]

For relatively flat $n_e(r)$ profiles ($L_n \gtrsim R/2$) and $s = rq'/q \simeq 1$ formula (4) gives $L_{\text{crit}} \simeq 0.08R$ at the $q = 2$ surface. The T_i/T_e dependence of formula (4) is considerably weaker than that in Eq. (2) leading to less sharp core $T_i(r)$ gradient. Undoubtedly, future studies will continue to refine and modify the formulas for χ_i and $L_{T_i,\text{crit}}$.

Tajima and his collaborators have emphasized the importance of $L_{T_i,\text{crit}}$ and the relaxation of the global ion temperature profile toward the critical profile as observed both in the large tokamaks[1] and in the global numerical simulations with the Toroidal Particle Code called TPC.[9] Due to the extended radial structures the profile establishes a constant $\mu = R/L_{T_i}$. In Fig. 1 we show the $L_{T_i}/R \simeq 0.1$ constant region reported in discharge 17110 in JT60-U at time $t_4 = 5.55\,\text{sec}$ in frame (b). In frame (a) of Fig. 1 we show the corresponding density profile which does not establish a constant L_n value. Other tokamaks[16] also show this exponential profile $T_i \propto \exp(-r/L_{T_i})$ with a well-defined L_{T_i}/R in the range of 0.1 to 0.2. The global toroidal particle simulations provide an explanation for this behavior. The simulations shows that the drift modes on neighboring rational surfaces are phase-locked together providing an overall global toroidal eigenmode. The two-time potential correlation function $\overline{\varphi(r,t)\varphi(r,t+\tau)}$ shows a well-defined eigenfrequency $\omega_k \approx \omega_{Di} = -2\varepsilon_n \omega_{*e}(T_i/T_e) =$ constant over the radial range $r/a \cong 0.1$ to 0.8. The radial correlation length Δr appears to be of order and scale as $\Delta r \cong 4(\rho_i a)^{1/2}$ as given by second order (envelope) ballooning mode theory. The radial structures shown in Fig. 2a are tilted in the $r-\theta$ plane due to the form of the ballooning wave function $F(r/\Delta r)\exp[in(q(r)\theta-\phi)-i\omega t]$ giving constant phase fronts rotating at the angular velocity $d\theta/dt=\omega/nq(r)$. Note how the modes become "disconnected" on the inside as predicted by Coppi.[8] In Figs. 2(b) and (c) the stabilizing effect of a weak $\mathbf{E}_r\times\mathbf{B}$ shear flow is shown. This stabilization will be taken into account in Sec. III.

Let us introduce the gradient of the ion power balance equation over the region $\Delta\sim L_{T_i}\ll a$. In the presence of a transport barrier the width Δ of the transport barrier is defined by a region of high shear in the mass flow velocity. Let us first review the relaxation of the temperature gradient $\mu(t)$ in the presence of the turbulence $W(t)$ and auxiliary power density $P^i_E(r)$ injection in the absence of sheared mass flows. The power density profile for the JT60-U reference shot analyzed in this investigation is shown in Fig. 3.

In the absence of sheared flows, the dynamics of $W(t)$ and $\mu(t)$ over the region Δ is given by

$$\frac{dW}{dt}=2\left[\gamma_0(\mu-\mu_c)-\gamma^{n\ell}W\right]W \tag{5}$$

$$\frac{d\mu}{dt}=\varepsilon^2\left(-\frac{\chi_0W\mu}{\Delta^2}+p'_E\right) \tag{6}$$

where $\gamma_0=2\varepsilon_n$, $\gamma^{n\ell}=\langle k_x^2\rho_i^2\rangle=(s/q),\varepsilon=(\rho_i/a)$, $\chi_0=(\rho_s/L_n)(cT_e/eB)$ and $p'_E=-(r/T_i)\partial_r(2P_E/3n_i)$. The time units in Eqs. (5) and (6) are L_n/c_s, and the ε^2 in Eq. (6) takes into account the slow transport time scale. The flow given by $\dot W,\dot\mu$ takes all initial states to the relaxed state parameterized by the gradient of the power deposition p'_E. The near-to-critical states are given by

$$W(p'_E)=\frac{\gamma^0}{2\gamma^{n\ell}}\left[\left(\mu_c^2+\frac{4\gamma^{n\ell}p'_E}{\gamma^0\chi_0}\right)^{1/2}-\mu_c\right] \tag{7}$$

$$\mu(p'_E)=\frac{1}{2}\left[\left(\mu_c^2+\frac{4\gamma^{n\ell}p'_E}{\gamma^0\chi_0}\right)^{1/2}+\mu_c\right]. \tag{8}$$

The curves $W(p'_E)$ and $\mu(p'_E)$ define a small, critical power injection rate p_E^* such that for $p'_E < p_E^* \equiv \chi_0\gamma^0\mu_c^2/4\gamma^{n\ell}$ the deviation from marginal stability is linear in the injection power and the confinement drops sharply from its ohmic value. For $p'_E > p_E^*$ the deviation from the critical gradient increases as $\mu = \mu_c(\gamma^{n\ell}p'_E/\gamma^0\chi_0)^{1/2}$ and the thermal diffusivity increases with the geometric mean of the local microscopic transport rate given by $\chi_0\gamma_0\mu_c/\gamma^{n\ell} = \chi^{\rm CHT}$ and the global pseudo diffusivity created by the heating $\Delta^2 p'_E$ rate over the region Δ.

In the regime $p'_E > p_E^*$ we have from $\chi = (\chi_0\gamma_0 p'_E\Delta^2/\gamma^{n\ell})^{1/2} = (\chi_{\rm CHT}\Delta^2 p'_E)^{1/2}$ the ion energy replace time $\tau_E = a^2/\chi_i$ given by

$$\tau_E = \left(\frac{s}{q}\right)^{1/2}\left(\frac{R}{a}\right)^{1/2}\left(\frac{\rho_i}{a}\right)^{\frac{\alpha-1}{2}}\left(\frac{a^2Bn}{RP_i}\right)^{1/2} = n^{\alpha_n}\, I_p^{\alpha_I}\, R^{\alpha_R}\, a^{\alpha_a}\, B^{\alpha_B}\, P_E^{-1/2} \tag{9}$$

where $\alpha_n = 1/2$, $\alpha_I = 1/2$, $\alpha_R = 1/2$, $\alpha_a = -\alpha/2$, and $\alpha_B = (1-\alpha)/2$. Here α is the macroscale dependence of the radial correlation length with $0 \le \alpha \le 1$. The importance of P_E and the gradient of P_E in the confinement scaling as developed here is consistent with the confinement behavior developed by Park, Bell, Tang,*et al.*[17] The explicit ρ_i/a scaling for $\alpha > 0$ in Eq. (9) is a reflection of the long correlation length in the global discription of the fluctuations. That systems not far from criticality develop long-range correlations is one of the important results of the field of research called self-organized criticality or 'SOC' theory.[18,19]

This dynamical model (Eqs. (5) and (6)) for the relaxation of the ion temperature profile toward the critical profile is the "critical gradient model" of Kishimoto *et al.*[20]

III. ENERGY-MOMENTUM TRANSPORT

In the presence of drift wave turbulence with $\mathbf{E}\times\mathbf{B}$ velocity fluctuations $\tilde{\mathbf{v}}$ of order the diamagnetic drift speeds $v_d = c_s\rho_s/L_n$ to $v_{di} = \rho_i v_i/L_{Ti}(\sim$ km/s) the ion energy-momentum transport equations contain both collisional and turbulent fluxes. The fluctuations and the fluxes are strongly influenced by both the magnetic shear in the toroidal field $\mathbf{B} =$

$\mathbf{B}_T + \mathbf{B}_p = RB_T\nabla\zeta + \nabla\zeta \times \nabla\chi$ (where $d\chi = B_pRdr_\perp$) and the shear in the mean mass flow $\mathbf{u} = u_\parallel\widehat{\mathbf{b}} + u_\perp\widehat{\mathbf{b}} \times \nabla\chi/|\nabla\chi|$. There are two surface functions associated with $u_\parallel$ and $u_\perp$ and the *shear* $u'_\parallel$ and $u'_\perp$ in these two surface functions have a strong effect on the stability and transport. The surface functions are determined by radial force balance and the condition of incompressibility $\nabla \cdot \mathbf{u} = 0$ for the mean mass flow.

The sheared mass flows $u'_\perp$ and $u'_\parallel$ break the symmetry of the drift-wave eigenmodes shifting the peak of the functions off the mode rational surfaces ($k_\parallel = 0$). The shifted eigenmodes produce finite quasilinear momentum fluxes $\langle\widetilde{v}_x\widetilde{v}_y\rangle$ and $\left\langle\widetilde{v}_x\widetilde{v}_\parallel\right\rangle$. The effect of $u'_\parallel$ is destabilizing and adds to the drive from η_i.[21] Here we consider the effects associated with perpendicular (poloidal) momentum transport which produces an acceleration proportional to the turbulence level and the symmetry breaking shear-flow $u'_\perp$. The relationship between $u'_\perp, u'_\parallel$ and the poloidal and toroidal shears are shown in Table I.

We measure the turbulence $\widetilde{v}$ in units of v_{de} rather than v_{di} due to the relatively fixed values of L_n and T_e in the transport barrier experiments. With $W = (\frac{L_n^2}{\rho_s^2})\sum_{\mathbf{k}}|e\phi_{\mathbf{k}}/T_e|^2$. We can summarize the quasilinear transport calculations[22] and the drift wave turbulence simulations of Su *et al.*[23] by writing

$$\partial_x\left\langle\widetilde{v}_x\widetilde{v}_y\right\rangle = v_dWu'_\perp \tag{10}$$

$$\partial_x\left\langle\widetilde{v}_x\widetilde{T}_i\right\rangle = -\frac{\rho_scT_e}{L_neB}W\frac{dT_i}{dx} \tag{11}$$

and

$$\frac{dW}{dt} = \frac{c_s}{L_n}\left(\gamma_0(\mu_i - \mu_c) - \gamma_s(u'_\perp)^2 - \gamma^{n\ell}W\right)W \tag{12}$$

where from HCT $\gamma^{n\ell} = \langle k_x^2\rho_s^2\rangle \simeq s/q$. From Su *et al.*[23] and Waelbroeck *et al.*[24] we have $\gamma_s \cong 0.5(L_s/c_s)^2$ and we take $\gamma^\ell = \gamma_0(\mu - \mu_c)$ where $\mu = R/L_T$ and μ_c is given by either Eq. (2) or Eq. (4). In the absence of shear flow Eq. (12) gives the L-mode turbulence level of $W_L = \gamma_0(\mu - \mu_c)/\gamma^{n\ell}$ and with Eq. (11) the $\chi_L = (\rho_s/L_n)(cT_e/eB)[(\gamma_0(\mu - \mu_c)/\gamma^{n\ell})]$. This

This is the form of χ that leads to formulas (7), (8), and (9).

The collisional transport of momentum in the banana regime defined by $\nu_{*i} = qR\nu_i/v_i\epsilon^{3/2} < 1$ produces the poloidal damping $\nu_{nc} = (\nu_i/\epsilon^{3/2})/(1+\nu_{*i}) = (v_i/qR)(\frac{\nu_{*i}}{1+\nu_{*i}})$ where $\epsilon^{1/2} = (r/R)^{1/2}$ arises from the trapped ion fraction and ν_i/ϵ from the effective trapped scattering rate. For the transport barrier region of JT60-U the momentum decay rate $\nu_{nc} \sim 300/\mathrm{s}$ is low compared to the turbulent momentum transport rate of $(v_{de}W/\Delta)$ where Δ is the width of the steep gradient region of the mass flow, i.e. the width of the transport barrier.

The momentum transport equation containing both the collisional and turbulent transport is of the form

$$\dot{u}_\perp = -\nu_{nc}(u_\perp - u_{nc}) - \partial_x \langle \widetilde{v}_x \widetilde{v}_y \rangle + \frac{P_\perp}{m_i n_i} \tag{13}$$

where the local momentum injection density from auxiliary heating is $P_\perp$. In writing Eq. (13) we have dropped $u_\parallel$ effects and the Pfirsch-Schlüter-inertial loading factor $1+2q^2$ and other details contained in Su *et al.*[23] The turbulent viscosity from Eq. (10) is negative due to the inverse cascade of the 2D turbulence. The negative viscosity generates large scale shear flows that suppress the thermal flux in Eq. (11) and improve the confinement of momentum, giving rise to the internal transport barrier formation.

The neutral beam injection (NBI) in JT60-U has multiple beam lines with both tangential and near-perpendicular beam line directions. Thus there is control over both the energy deposition profile $P_E(r)$ and the momentum deposition profile $P_\perp(r)$. The local power profile $P_E(r)$ is known and has a strong radial gradient. For the local transport analysis carried out here it is important to recognize that it is the *gradients* of P_E^i/n_i and $P_\perp/m_i n_i$ that drive the gradients of T_i and $u_\perp$. Thus, we must take the gradients of the local balance equations, or equivalently introduce $x = r - r_{tb}$ where we take the projections required $\int_{-\Delta/2}^{\Delta/2} dx\, x(\text{transport equations})/F(n,T) = 0$ where $F(n,T)$ are suitable weighting functions to obtain the local dynamical equations for $\mu(t) = R/L_{Ti}(t)$ – the gradient parameter and

$F(t) = \Delta^2 u_\perp'^2(0)/12c_s^2$ the shear flow parameter. The procedure is described in more detail for the resistive-g transport-shear flow problem in Sugama and Horton.[25]

From the projection for the gradient parts of the radial transport equations over the transport barrier width Δ, we obtain the following dynamical equations for the transport state variables $W(t), \mu(t)$, and $F(t)$. Repeating Eq. (12) in time units of L_n/c_s we have

$$\frac{dW}{dt} = \Big(\gamma_0(\mu - \mu_c) - \gamma_p F - \gamma^{n\ell} W\Big)\, W \tag{14}$$

$$\frac{d\mu}{dt} = -\chi_0 W \mu + P_E' \tag{15}$$

$$\frac{dF}{dt} = (\gamma_p W - \nu) F + F^{1/2} P_\perp'. \tag{16}$$

The dynamics of these three driven damped dissipative equations is rich — describing three distinct transport states. The states are analyzed theoretically by determining the fixed points (FP) and their stability.

The dynamics leading to the formation of the transport barrier follows from the coupling between (14) and (16) as most easily seen by freezing $\mu - \mu_c$. First consider $P_\perp' = 0$ where the turbulence-generated flow shear creates a transport barrier in the form of an L$\rightarrow$H. This transition occurs as an *exchange of stability* of the L-mode fixed point ($W = W_L = \gamma^\ell/\gamma^{n\ell}, F_L = 0$) and the H-mode fixed point ($W_H = \nu/\gamma_p,\ F_H = [\gamma^\ell - (\gamma^{n\ell}\nu/\gamma_p)]/\gamma_p$). The exchange of stability occurs when the collisionality drops through the critical value

$$\nu_{nc} < \nu_{nc}^* = \frac{\gamma^\ell}{\gamma^{n\ell}}\gamma_p \approx \frac{v_d(\mu - \mu_c)}{L_E(s/q)} \tag{17}$$

where $L_E \sim \Delta$ is the width of the shear flow layer. For $P_\perp' \neq 0$ the transition from stable L-mode to a stable H-mode is easier. We determine the condition on $P_\perp'$ below where we include both P_E', which degrades confinement, and $P_\perp'$ which improves confinement.

In the absence of sheared flows ($F \equiv 0$) the system (14) and (15) is the critical gradient model that determines the degree to which the auxiliary heating pulls the gradient above the threshold of instability μ_c and how the turbulence level grows to provide power balance. For the $(\dot{W}, \dot{\mu})$ flow on the $F = 0$ plane there are only the attracting fixed points parameterized by P'_E. The stable, attracting L-mode confinement states are given in Eqs. (7) and (8) as a function of the microscopic transport parameters and the macroscopic driving power for large power $P'_E > P^*_E$ the turbulence grows as $W \simeq (P'_E W_L/\chi_0 \mu_c)^{1/2}$ and $\chi = (\chi_i L_T^2 P_E/nT_e)^{1/2}$ is the geometric mean of χ_i and $L_T^2 P_E/nT_e$. Thus, the self-consistent transport is a function of both the *microscopic transport* and the *driving power* along with degree of peaking. This result is entirely consistent with L-mode "confinement" studies.[17]

In the general case there is clearly a competition between the increase of χ_i with $(P'_E)^{1/2}$ and the decrease of χ_i due to the momentum gradient $P'_\perp$ that drives the formation of a transport barrier. The fixed points in W are now determined by the fourth-order polynomial which has three real roots $W_H^s < W_H^{us} < W_L^s$ where the intermediate H-mode root (W_H^{us}) is unstable. The polynomial for the fixed points is

$$\left(\frac{\gamma^0 P'_E}{\chi_0 W} - \gamma^0_{\mu c} - \gamma^{n\ell} W\right)\left(\nu_{nc} - \frac{v_d}{L_E W}\right)^2 = \frac{L_s^2}{L_E^2}(P'_\perp)^2 \tag{18}$$

and the stability conditions must be determined numerically. For weak $(P'_\perp)^2$, however, the important transition condition from the $(P'_\perp = 0)$ H-mode with $W = W_H = \nu_{nc} L_E/v_d$ to the *super-suppressed transport* (SST) regime is found by letting

$$W = W_H w$$

and taking $W_H \ll W_L$ and $P'_E \gg (\mu_c W_H \chi_0)$. The roots of Eq. (18) are then controlled by the effective control parameter

$$p_{\text{eff}} = \frac{L_s^2}{L_E^2}\left(\frac{P'_\perp}{\nu_{nc}}\right)^2 \left|\frac{\chi_0 L_E \nu_{nc}}{\gamma^0 v_d P'_E}\right|. \tag{19}$$

When $p_{\text{eff}} > 1$ the confinement enters the super-suppressed transport regime. In terms of p_{eff} the turbulence drops according to

$$W = W_H\left(\frac{2}{2 + p_{\text{eff}} + \sqrt{4p_{\text{eff}} + p_{\text{eff}}^2}}\right) \tag{20}$$

going to a very low level for $p_{\text{eff}} \gg 1$. In deriving Eq. (20) we have used that $w = W/W_H \lesssim 1$ to reduce Eq. (18) to $(w^{-1} - 1)(1 - w) = p_{\text{eff}}$.

In this (SST) regime the gradient becomes very steep with $\mu - \mu_c \simeq P'_E/\chi_0 W$ and the system is maintained at linear marginal stability $\gamma^\ell = \gamma_0(\mu - \mu_c) - (L_s u'_\perp/c_s)^2 \approx 0$ by the strong shear flow driven by $P'_\perp$ and damped by the neoclassical viscosity.

Formation of a steep gradient controlled by near perpendicular momentum injection is shown in Fig. 4 from Koide *et al.*[1] In Fig. 4(a) during the period labelled I there is the self-consistent rise of a steep ∇T_i along with a drop of χ_i shown in 4(b) in the region $\Delta = 0.1\,\text{m}$ layer around $r/a = 0.7$.

The prediction contained in the new parameter $p_{\text{eff}} \propto (p'_\perp)^2/p'_E$ that the perpendicular momentum $p'_\perp$ can overcome the degradation of confinement from p'_E is a key conclusion from the coupled thermal energy and momentum balance equations. The essential physical effect is the suppression of the growth rate and the turbulence by sheared perpendicular flows. This shear flow effect is well documented with computer simulations.[20,23,25,26] The experimental manifestation of local stabilization and the creation of a super-suppressed transport zone has been achieved in PBX-M.[27,28] In this experiment the application of 2MW of IBWH heating in an NBI driven plasma is sufficient to create core H-mode with a high ion temperature producing a neutral flux signature and a high ion temperature gradient that would be unstable without the shear flow layer driven by the IBWH localized heating.

IV. CONCLUSION

The analysis of the energy-momentum transport equations presented here shows that the self-consistent nature of the interactions of the turbulence with driving and stabilizing forces of the ion temperature gradient and the sheared ion mass flows leads to a variety of self-organized confinement regimes. By including both the gradient of the local power deposition and the local momentum deposition from the auxiliary ion heating sources (NBI, IBWH) as control parameters in the driven-dissipative transport equations we are able to derive three confinement regimes, the three regimes are identified with the L-mode, the H-mode, and a super-suppressed transport regime. The bifurcations are studied. The conditions on the neoclassical viscosity, the microscopic anomalous transport parameters and the external control parameters are derived for the bifurcation points between the regimes. The conditions derived for the transitions appear to correlate well with the conditions used in JT60-U with the multiple tangential and perpendicular NBI lines and to those in PBX-M with the parallel NBI and local IBWH resonant absorption region for the formation of transport barriers.

The formation of transport barriers appears to be of fundamental importance in fusion confinement. The understanding of these barriers is derived directly following the procedures developed for the study of ion thermal transport from the early works of Coppi and his collaborators.

ACKNOWLEDGMENTS

The author appreciates contributions from J.Q. Dong, B. Dorland, T. Fukuda, M. Kotschenreuther, M. LeBrun, H. Sharai, T. Tajima, and F.L. Waelbroeck. This work is supported in part by the U.S. Dept. of Energy contract #DE-FG05-80ET-53088 and in part by Advanced Science Research Center at JAERI.

REFERENCES

[1] Y. Koide, M. Kikuchi, M. Mori, *et al.*, Phys. Rev. Lett. **72**, 3662 (1994).

[2] Y. Koide, S. Ishida, M. Kikuchi, M. Mori, S. Tsuji, T. Nishitani, Y. Kawano, T. Hatae, T. Fujita, T. Ozeki, H. Shirai, Y. Kamada, R. Yoshino, H. Ninomiya, M. Azumi, and the JT-60 Team, (15th International Atomic Energy Agency Conference, Sevilla, 1994).

[3] B. Coppi, M.N. Rosenbluth, and R.Z. Sagdeev, Phys. Fluids **10**, 582 (1967).

[4] W. Horton, R.D. Estes, and D. Biskamp, Plasma Physics **22**, 663 (1980).

[5] S. Hamaguchi and W. Horton, Phys. Fluids B **2**, 1833 (1990).

[6] S. Hamaguchi and W. Horton, Phys. Fluids B **2**, 3040 (1990).

[7] B. Coppi and F. Pegoraro, Nucl. Fusion **17**, 969 (1977), and B. Coppi, S. Migliuolo, and Y.-K. Pu, Phys. Fluids B, 2322 (1990).

[8] B. Coppi, Phys. Rev. Lett. **39**, 939 (1977).

[9] M.J. LeBrun, T. Tajima, G. Furnish, and W. Horton, Phys. Fluids (1993).

[10] S.E. Parker, W.W. Lee, and R.A. Santoro, Gyrokinetic simulation of ion temperature gradient driven turbulence in 3D toroidal geometry, Phys. Rev. Lett. **71**, 2042 (1993).

[11] J.-Y. Kim and W. Horton, Phys. Fluids B, (1991).

[12] W. Horton, D.-I. Choi, and W. Tang, Phys. Fluids B, (1981).

[13] J.-Y. Kim and W. Horton, "Ion temperature gradient driven transport" AIP Conf. No. 284 (1994).

[14] Romanelli, Phys. Fluids B **1**, 1018 (1989).

[15] W. Dorland, M. Kotschenreuther, J.Q. Dong, W. Horton, F.L. Waelbroeck, T. Tajima, M.J. LeBrun, M.A. Beer, R.E. Waltz, and R.R. Dominguez, Plasma Phys. Contr. Fusion (International Atomic Energy Agency, 1994).

[16] W. Horton, D. Lindberg, J.-Y. Kim, J.Q. Dong, G.W. Hammett, S.D. Scott, M.C. Zarnstorff, and S. Hamaguchi, Ion temperature gradient driven transport in a density modification experiment on the TFTR tokamak, Phys. Fluids B **4**, 953 (1992).

[17] H.K. Park, M.G. Bell, W.M. Tang, G. Taylor, M. Yamada, R.V. Bundy, D.C. McCune, and R. Wieland, Nucl. Fusion (1994).

[18] T. Hwa and M. Kardan, Phys. Rev. Lett. **62**, 1813 (1989).

[19] P. Bak, C. Tang, and K. Wiesenfeld, Phys. Rev. Lett. **59**, 381 (1987) and **60**, 2347 (1988).

[20] Y. Kishimoto, T. Tajima, M.J. LeBrun, J.-Y. Kim, W. Horton, S. Tokuda, F.L. Waelbroeck, and T. Fukuda, 15th Conf. (International Atomic Energy Agency, 1994).

[21] J.Q. Dong and W. Horton, Kinetic quasi-toroidal ion temperature gradient instability in the presence of sheared flows, Phys. Fluids B **5**, 1581 (1993).

[22] J.Q. Dong, W. Horton, R.D. Bengtson, and G.X. Li, Momentum-energy transport from turbulence driven by parallel flow shear, Phys. Plasmas, December (1994).

[23] X.-N. Su, P.N. Yushmanov, J.Q. Dong, and W. Horton, Shear flow generation from the interaction of neoclassical and drift wave transport processes, Phys. Plasmas **1**, 1905 (1994).

[24] F.L. Waelbroeck, J.Q. Dong, W. Horton, and P.N. Yushmanov, Phys. Plasmas **1**, 3742 (1994).

[25] H. Sugama and W. Horton, Plasma Phys. Contr. Fusion **37**, 345 (1995).

[26] S. Hamaguchi and W. Horton, Phys. Fluids B **4**, 319 (1992).

[27] M. Ono, *et al.*, 15th Conf. (International Atomic Energy Agency, Seville, Spain 1994).

[28] B. LeBlanc, M. Ono, and Okubagashi, *et al.*, "Core H-mode in PBX-M," to appear in the Phys. Plasmas, 1995.

FIGURE CAPTIONS

Fig. 1. The time evolution of the density $n_e(r,t)$ and ion temperature $T_i(r,t)$ profiles in the discharge 17110 in JT60-U. On the right-hand side are the two key stability parameters computed for the first and last time values. Note in (b) the relatively constant value of L_{T_i}/R near 0.1 indicating a global exponential ion temperature profile as observed in the toroidal particle simulations.

Fig. 2. Equipotential profiles obtained from the global particle code TPC shown near the time of saturation for three cases. (a) without external mass shear flow, (b) with a weak $\mathbf{E}_r \times \mathbf{B}$ shear flow in the ion diamagnetic direction, and (c) the same weak shear flow now in the electron diamagnetic direction.

Fig. 3. Power deposition $P_E(r)$ function for the JT60-U discharge 17110. The radial gradient associated with $P_E(r)$ forms an external control parameter in Eqs. (6) and (15).

Fig. 4. Formation of a transport barrier. (a) Space-time evolution of the ion temperature $T_i(r,t)$ for discharge 17110 with the insert showing the associated shear flow measured from Doppler shifted impurity radiation lines. (b) The time dependence of the power balance $\chi_i^{\rm PB}$ thermal diffusivity for the radial region $\Delta = 0.1\,\rm m$ at the transport barrier $r_{tb}/a \simeq 0.7$.

Table I: SHEAR-FLOW PARAMETERS

Non-Uniform Doppler Shift from ion shear flow $\mathbf{u}(\mathcal{X}, t)$

$$\mathbf{k} \cdot \mathbf{u} = k_\perp u_\perp + k_\| u_\| = \frac{m}{r} u_\theta + \frac{\ell}{R} u_\phi$$

$$\frac{d}{dx} (\mathbf{k} \cdot \mathbf{u}) = m \left(\frac{u_\theta}{r} \right)' + \ell \left(\frac{u_\phi}{R} \right)'$$

For ballooning modes $k_\| \cong 0$ then $\ell = m/q$

$$= m \left(\frac{u_\theta}{r} \right)' + \frac{m}{q} \left(\frac{u_\phi}{R} \right)'$$

Thus the parallel-perpendicular shears are given by

$$u'_\perp \leftrightarrow r \left(\frac{u_\theta}{r} \right)' + \frac{r}{q} \left(\frac{u_\phi}{R} \right)'$$

$$u'_\| \leftrightarrow \frac{du_\phi}{dr}$$

In Transport Barriers the range is 10^5 to 7×10^5/s

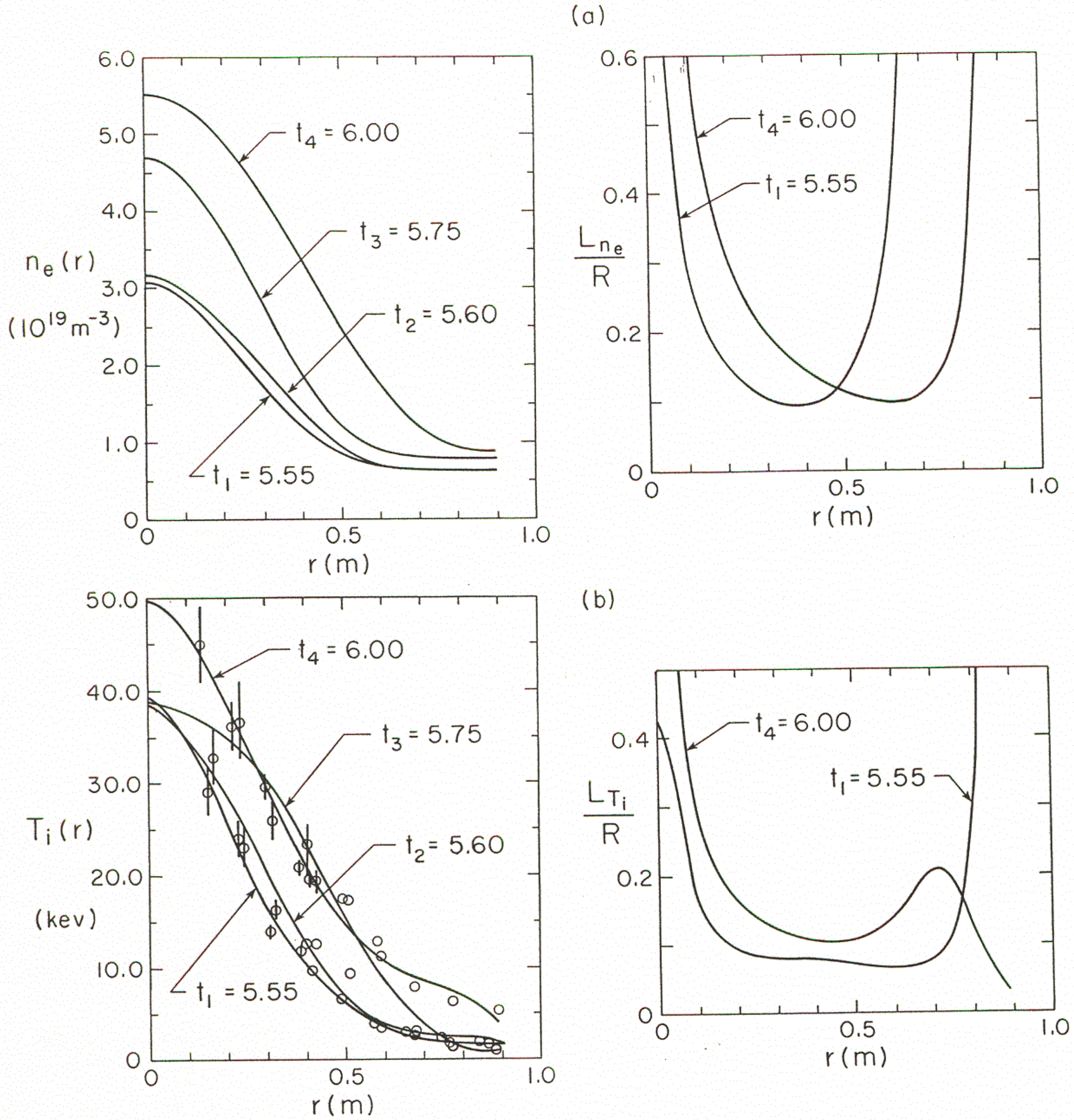

(a)
$n_e(r)$ ($10^{19}m^{-3}$)
$t_4 = 6.00$
$t_3 = 5.75$
$t_2 = 5.60$
$t_1 = 5.55$
r (m)
$\frac{L_{n_e}}{R}$
$t_4 = 6.00$
$t_1 = 5.55$
r (m)
(b)
$T_i(r)$ (kev)
$t_4 = 6.00$
$t_3 = 5.75$
$t_2 = 5.60$
$t_1 = 5.55$
r (m)
$\frac{L_{T_i}}{R}$
$t_4 = 6.00$
$t_1 = 5.55$
r (m)

Fig. 1

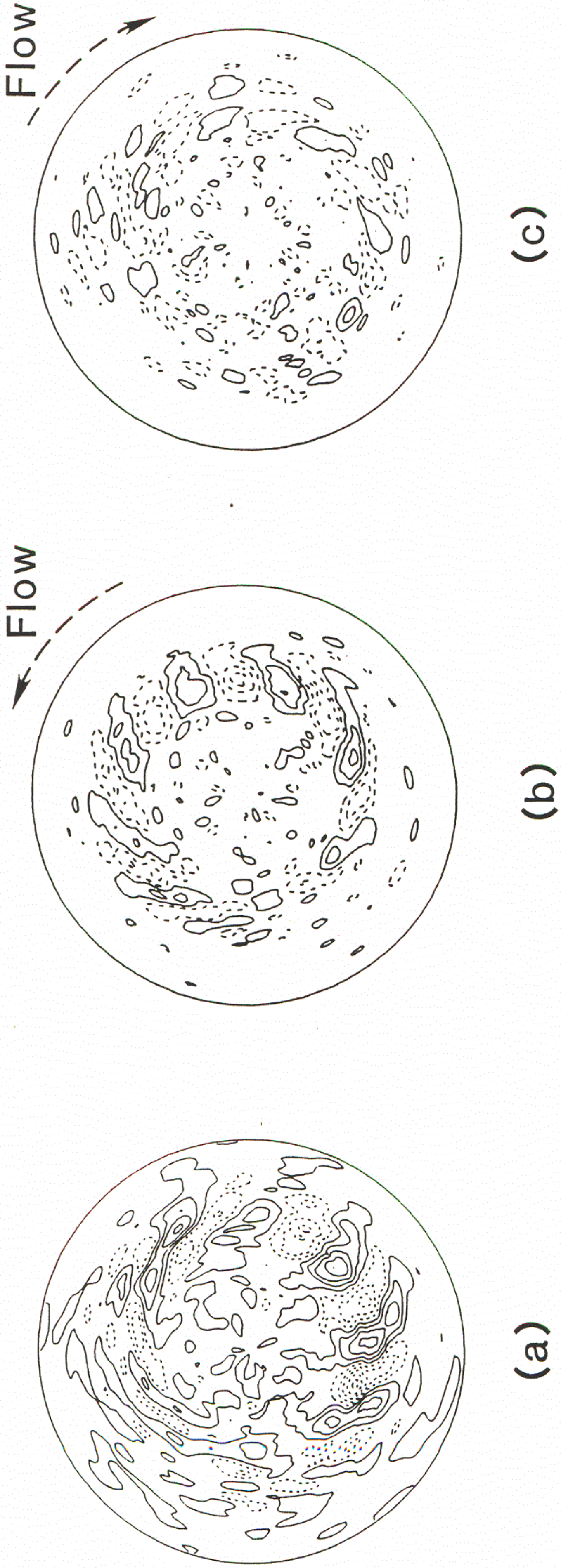

Fig. 2

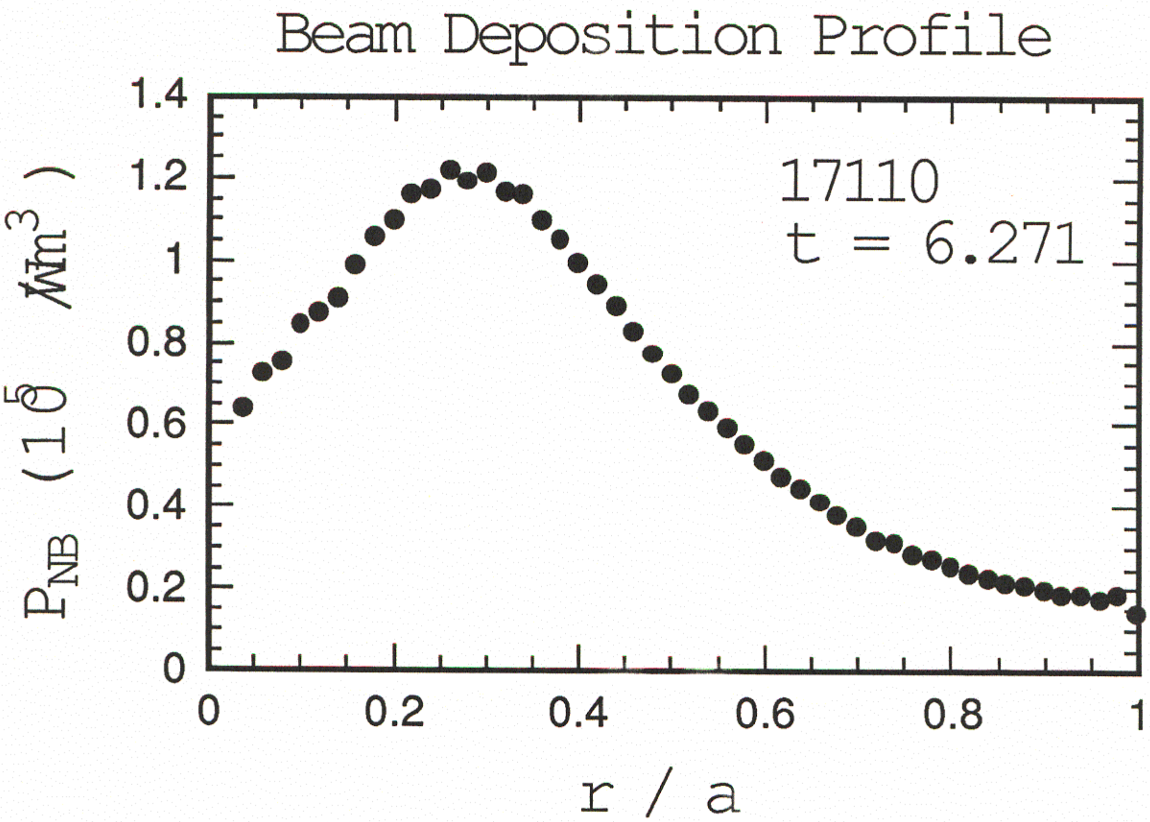

Beam Deposition Profile
17110
t = 6.271
P_NB (10^5 W/m^3)
r / a
0
0.2
0.4
0.6
0.8
1
1.2
1.4

Fig. 3

JT-60 Tokamak Profiles
Internal Transport Barrier

- $\tau_d < \tau_{\nabla T_i}$
  Duration of steep ∇T_i $\quad\quad \tau_{\nabla T_i} \sim 150$ ms
  Time constant of heat diffusion $\quad\quad \tau_d \equiv 1.5 L_{T_i}^2/\chi_i \sim 12$ ms

- Reduction in χ_{eff}

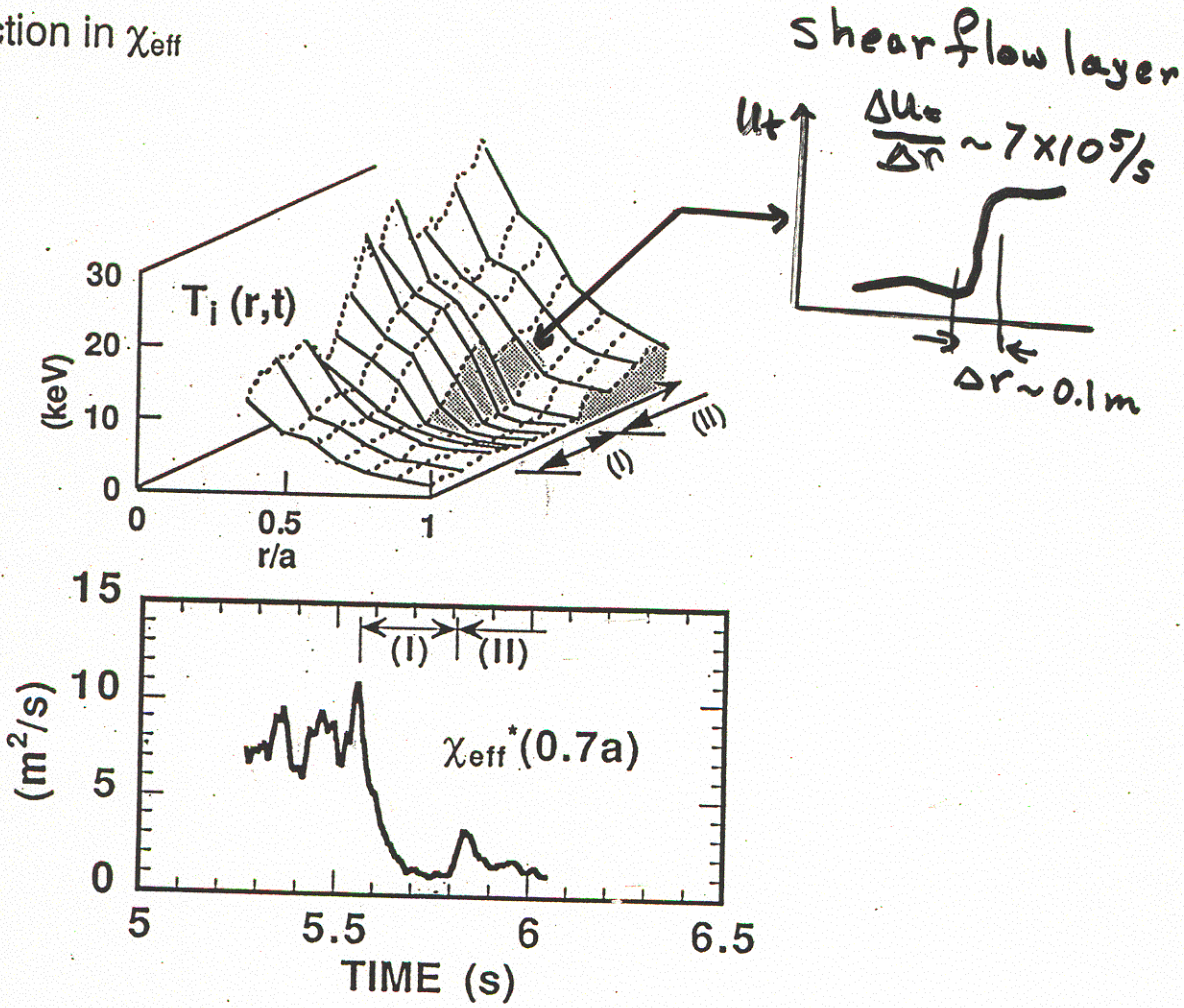

Fig. 4